Theoretical Prediction of Magnetism in C-doped TlBr

Yuzhi Zhou, E. E. Haller, and D. C. Chrzan
Materials Sciences Division, Lawrence Berkeley National Laboratory, Berkeley, California 94720, USA
and Department of Materials Science and Engineering, University of California at Berkeley, Berkeley, California 94720, USA
(Received 7 March 2014; revised manuscript received 15 April 2014; published 9 May 2014)

We predict that C, N, and O dopants in TlBr can display large, localized magnetic moments. Density functional theory based electronic structure calculations show that the moments arise from partial filling of the crystal-field-split localized p states of the dopant atoms. A simple model is introduced to explain the magnitude of the moments.

DOI: 10.1103/PhysRevB.89.195201 PACS number(s): 75.50.Pp, 71.15.Mb, 71.55.−i, 75.10.−b

Dilute magnetic semiconductors (DMS) are appealing materials for applications in spintronics [1–5]. A new category of DMS is based on the magnetic moments from nonmagnetic *sp*-valent impurities in otherwise nonmagnetic oxide materials [6]. C-doped ZnO [7,8], N-doped MgO [9], and other N-doped alkaline earth metal oxides [10] have either displayed magnetism experimentally or have been predicted to be magnetic theoretically. Here it is argued that doping of non-oxide-based wide band gap semiconductors can lead to similar properties. More specifically, density functional theory (DFT) based electronic structure total energy methods predict that doping TlBr with C, N, and O can lead to the formation of local magnetic moments on the dopant atoms.

At room temperature, TlBr is stable in the CsCl structure. In this structure, TlBr is a semiconductor with an indirect band gap of 2.665 eV (measured at 2 K) and a direct gap of 3.013 eV (measured at 4 K) [11,12], values that DFT calculations employing hybrid functionals are able to reproduce [13]. The material is of interest because its band gap, its density, and the fact that it contains elements with high Z suggest that it can be a high-quality room temperature radiation detector material [14]. In fact, room temperature detectors based on TlBr have demonstrated energy resolutions as high as 2% [15]. Moreover, TlBr has been intentionally doped with a number of elements including Pb, Se, and C [16–18].

Electronic structure total energy calculations were performed using the plane-wave DFT code VASP [19]. The exchange and correlation energy was described by the generalized gradient approximation (GGA) proposed by Perdew, Burke, and Ernzerhof (PBE) [20]. Electron-ion interactions were treated with projector augmented wave (PAW) potentials [21]. All calculations were performed using a plane-wave basis with a 550 eV energy cutoff. The absolute convergence of the total energy with respect to the cutoff energy is better than 2×10^{-3} eV/atom. The convergence criterion for self-consistent field (SCF) loop is 1×10^{-5} eV. To simulate point defects, a supercell containing $3\times3\times3$ unit cells of CsCl structure TlBr (54 atoms in the undoped crystal) was used. The Brillioun zone was sampled using a $2\times2\times2$ Monkhorst-Pack k-point grid. Atomic positions and the supercell lattice vectors were relaxed until the maximum Hellmann-Feynman force on any atom was below 0.02 eV/Å. Spin-orbit coupling was included in all calculations. Results were spot-checked using the hybrid functional PBE0 [22] and a larger supercell with PBE functional in different defect systems (more information can be found in Sec. 1 of the Supplemental Material [23]). The calculated magnetic moments are close to those results reported here.

Three types of interstitial sites are shown in Fig. 1. The sites are referenced by their site symmetry. For example, the Tl-tetragonal site [Fig. 1(a)] sits at what would be the octahedral site of the body-centered-cubic (BCC) structure. However, because the atoms defining the cube-octahedron are not all identical, the tetragonal site symmetry is defined by the 4 Tl atoms at corners of the cubic plane and 2 Br atoms forming the point of the octahedron. A Br-tetragonal site is defined similarly [Fig. 1(b)]. The last type of interstitial site studied [Fig. 1(c)] has the symmetry C_{2v} and is referred to as a 2-fold site. This site would be the tetrahedral interstitial site of the BCC structure. Note that the described symmetries are those associated with a perfect crystal. Relaxation can reduce the symmetry.

The calculated magnetic moments for four different C defect geometries are shown in Table I. Except for the 2-fold site defect, all others show magnetic moments. In addition, all magnetic moments are near integral multiples of μ_B.

The site-projected density of states (DOS) and site-projected magnetization density plots for C at the Tl-tetragonal supercell are shown in Fig. 2. The site-projected DOS is the projection of total DOS onto s, p, and d states within a small sphere around each ion in the supercell. (The Wigner-Seitz radius of the sphere is chosen to be the default provided in the pseudopotential files for each ion.) In Fig. 2(a), the peak directly below the Fermi level (labeled 1) in total DOS has very large portion of C p states and a certain amount of s and p states from the nearest neighbor (n.n.) Tl ions. For other regions of the DOS plot, the projected DOS of C and n.n. ions are almost negligible compared to the total DOS. In addition, the number of states in peak 1 is 2, which is same as the number of C p electrons. In Fig. 3, the 2D view slicing through the Tl cubic plane and the 3D contour plot of the partial charge density distribution from the wave functions at Γ of the two states in peak 1 (also the two highest occupied states) are shown.

These two states have nearly identical charge densities, which is required by the symmetry (discussion of the symmetry of the wavefunction and partial charge density can be found in Sec. 2 of the Supplemental Material [23]). Thus only one of them is shown. They localize near the C atom with a small portion on n.n. ions, which indicates that peak 1 is mainly

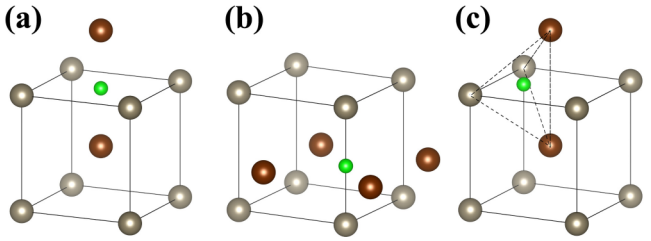

FIG. 1. (Color online) Three types of interstitial sites in TlBr: (a) Tl-tetragonal site, (b) Br-tetragonal site and (c) the 2-fold site. Tl ions are represented by light colored balls and Br ions are represented by dark colored balls. C atom is represented by a small light colored ball. We adopt the same representation in the following figures.

composed of 2 C p-states with slight hybridization of states from n.n. ions. Moreover, the charge density contour has the same symmetry as the local crystal environment (D_{4h}).

The site-projected magnetization density further reveals the contribution from the site-projected DOS to the magnetization density in $\boldsymbol{x}$, $\boldsymbol{y}$, and $\boldsymbol{z}$ directions, respectively. Figure 2(b) shows the site-projected DOS of C p states and its contribution to magnetization density in the $\boldsymbol{x}$ direction [m(C p, $\boldsymbol{x}$)]. m(C p, $\boldsymbol{y}$) and m(C p, $\boldsymbol{z}$) are similar in nature to m(C p, $\boldsymbol{x}$). The peak directly below and the peak right above the Fermi energy level (labeled 2 and 3) have opposite sign of magnetization density. This is similar to the spin-up and spin-down splitting in a spin-polarized calculation. Note that we refer peak 3 to the continuous interband states ranging from 3.0 eV to about 4.2 eV. The total site-projected magnetization density of C p states [m(C p, total)] is defined as the magnitude of vector $\boldsymbol{m}$(C p) = (m(C p, $\boldsymbol{x}$), m(C p, $\boldsymbol{y}$), m(C p, $\boldsymbol{z}$)). Figure 2(c) shows that m(C p, total) is very close to the number of projected DOS in peaks 2 and 3. This fact means these two peaks have been fully polarized, at least within the spheres of projection.

The distribution of total magnetization density in the $\boldsymbol{x}$ direction [this is the overall magnetization density in the supercell, not the m(C p, total) defined above] is shown in Fig. 4. The magnetization density also localizes near the C atom and looks very similar to those presented in Fig. 3. The above evidence leads to the conclusion that C p electrons make major contributions to the total magnetic moments through slight hybridization with n.n. ions.

This magnetic behavior can be understood using a simple crystal field model. The filling of the electrons into the levels split by the local crystal field follows Hund's first rule. The local symmetry of C at the Tl-tetragonal site after relaxation is D_{4h}. Under this symmetry, p_x and p_y orbitals, which are aligned along the $\boldsymbol{x}$ and $\boldsymbol{y}$ directions within the Tl cubic plane, transform according to a two-dimensional irreducible representation. The p_z orbital which is perpendicular to the Tl cubic plane transforms according to a one-dimensional irreducible representation. Three C p orbitals now split into

TABLE I. Magnetic moments of different C impurity defects in TlBr.

Defect configuration	Magnetic moments (μ_B)
Tl tetragonal	1.96
Br tetragonal	1.96
2-fold	0
C replacing Br	2.99

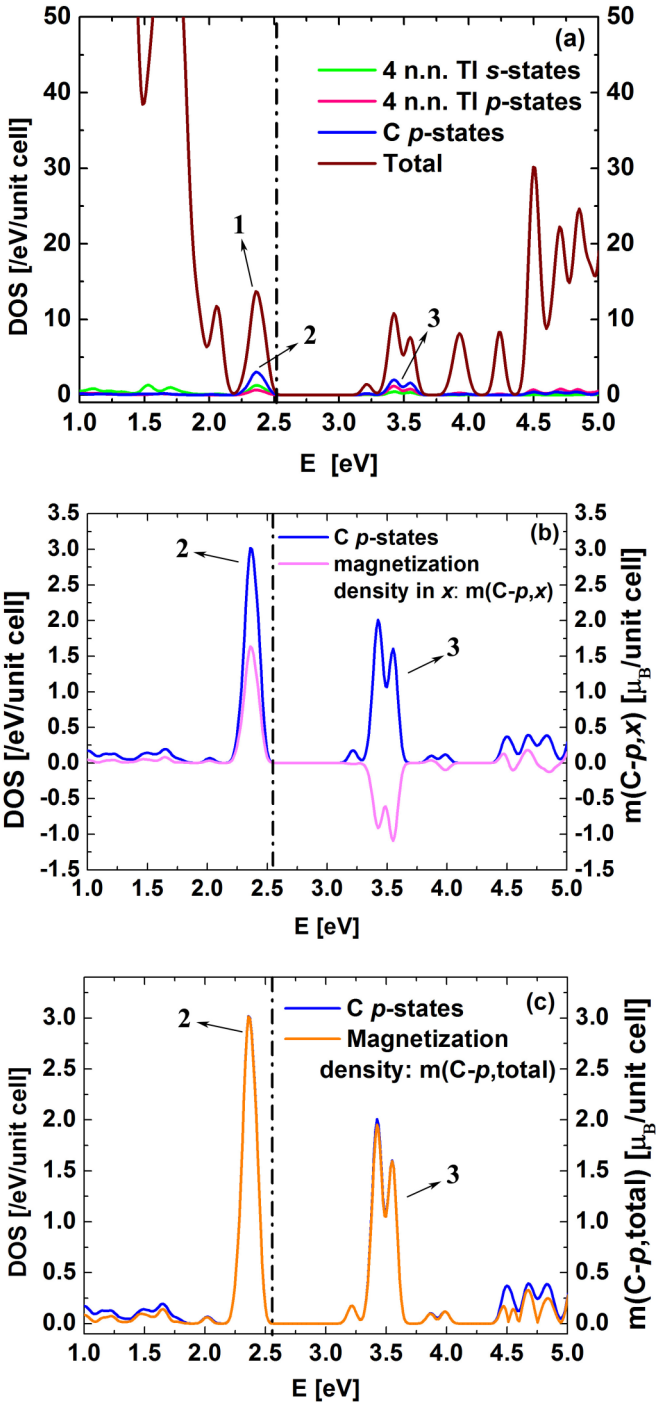

FIG. 2. (Color online) Site-projected DOS and magnetization density for C at Tl-tetragonal supercell. (a) Total DOS and site-projected DOS of C p states and 4 nearest-neighboring (n.n.) Tl s and p states. (b) Site-projected DOS of C p states and its magnetization density in the $\boldsymbol{x}$ direction [m(C p, $\boldsymbol{x}$); similar behavior for $\boldsymbol{y}$ and $\boldsymbol{z}$ directions]. The dashed line indicates the Fermi energy level. (c) Site-projected DOS and total site-projected magnetization density of C p states [m(C p, total)].

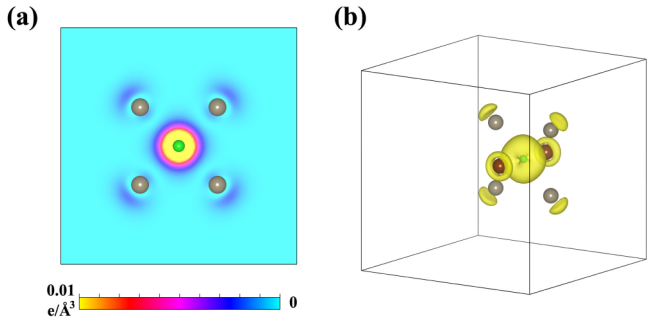

FIG. 3. (Color online) Partial charge density distributions of two highest occupied states at Γ in C at Tl-tetragonal system. The partial charge density distributions of two states are almost the same; thus only one is shown. (a) 2D view slicing through the Tl cubic plane and (b) 3D side view of the partial charge density contour. All other atoms are hidden (same in the following figures). The visualization program is VESTA [24].

a 2-fold degenerate level (p_x and p_y) and a 1-fold degenerate level (p_z). We then determine the correct ordering of the split levels by choosing the one which gives the correct amount of magnetization when 2 C p electrons fill these levels. To reproduce the calculated magnetic moments, the 2-fold level lies below the 1-fold level and is filled by 2 C p electrons with aligned spin. Since each spin contributes 1 μ_B to the moment, this configuration gives total 2 μ_B moments, close to the calculated value of 1.96 μ_B. The fact that the eigenstates of the 2-fold level are linear combinations of p_x and p_y orbitals is also consistent with the feature of the partial charge density distributions in Fig. 3 (mathematical details can be found in Sec. 2 of the Supplemental Material [23]).

We further studied the −1 charge state of C at the Tl-tetragonal site. The calculated magnetic moment is 1.01 μ_B. After the relaxation, the C atom, which locates at the center of the Tl cubic plane in the previous case, now is displaced out of the plane, as shown in Fig. 5(a). The local relaxed symmetry now becomes C_{2v} but is very close to C_{4v} (the four n.n. Tl ions form a rectangle which is very close to a square). Thus the p states split into three 1-fold levels with two of them very close to each other. Compared to Fig. 3, the partial charge density of the extra electron now has uneven distribution on n.n. Br and Tl ions and a distorted bilobed

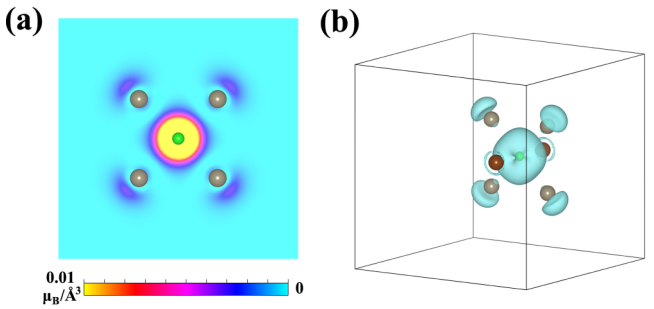

FIG. 4. (Color online) Distribution of total magnetization density in $\boldsymbol{x}$ direction: (a) 2D view slicing through the Tl cubic plane and (b) 3D side view of the contour plot. Similar behaviors are found for the $\boldsymbol{y}$ and $\boldsymbol{z}$ directions. The contour is plotted with a different color to be distinguished from charge density contours.

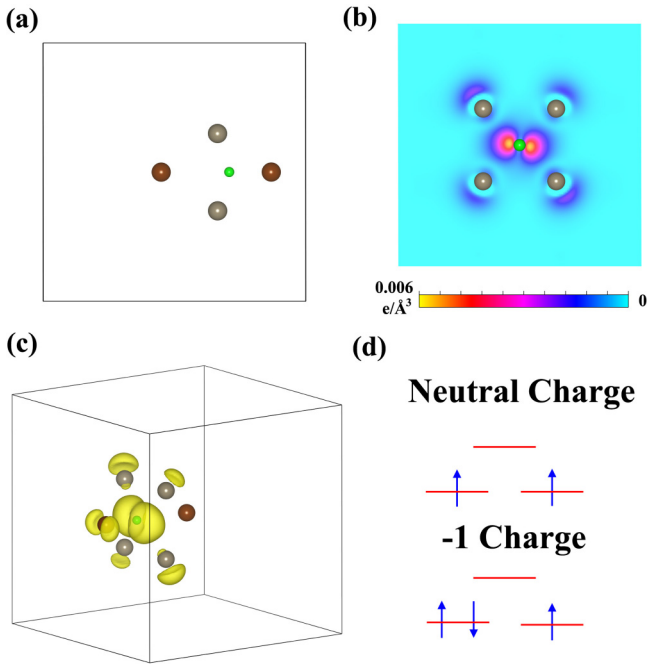

FIG. 5. (Color online) (a) Relaxed atomic configuration of −1 charge state of C at Tl-tetragonal site. C atom is displaced out of the 4 Tl-ion plane. (b) 2D view slicing through the 4 Tl-ion plane and (c) 3D side view of partial charge density contour of the highest occupied state. (d) The electron filling diagram of neutral and −1 charge state. In the −1 charge state diagram, the doubly occupied level is slightly higher than the singly occupied level due to the on-site repulsion between the electrons occupying it.

distribution around the C atom, as shown in Figs. 5(b) and 5(c). The electron filling diagrams for neutral and −1 charge state are shown in Fig. 5(d). Compared to neutral charge system, the added electron fills one of the 2-fold levels with opposite spin of previous two electrons. Then the Coulomb repulsion between the two opposite-spin electrons slightly raises this level and distorts the local environment from D_{4h} to C_{2v}. This leads to a diagram with the doubly occupied level slightly higher than the singly occupied level. The model gives 1 μ_B of magnetic moment which again is in excellent agreement with the calculated value of 1.01 μ_B.

We investigated other dopants as well, and the results are shown in Table II. The electron filling diagrams are shown in Fig. 6 to illustrate all the cases in Table II and two cases (C at

TABLE II. Local symmetry and magnetic moments for other defect configurations.

Initial defect configuration	Charge state	Local symmetry[a]	Magnetic moments (μ_B)
C at 2-fold	+1	C_{2v}	0.99
N at 2-fold and Tl tetragonal	0	C_{2v}	1.00
N at 2-fold	−1	C_{4v}	0
O replacing Br	0	O_h	0.99
O at Tl tetragonal	0	D_{4h}	0

[a]Here, the local symmetry is determined by the defect configuration after relaxation.

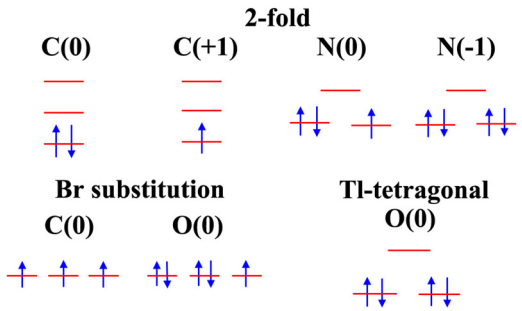

FIG. 6. (Color online) Electron filling diagrams to explain the magnetic moments in Table I and Table II. The headings indicate the site of the defect. The numbers in brackets indicate the charge states.

Tl-tetragonal site and C replacing Br) in Table I. For N at the 2-fold and N at the Tl-tetragonal site, even though their initial configurations are different, they all relaxed to the same final geometry with C_{2v} symmetry. Therefore, only one electron filling diagram is used. This diagram is also similar to that of the -1 charge state of C at the Tl-tetragonal site with doubly occupied level slightly higher than the singly occupied level. From Fig. 6, we can see that the crystal field splitting model explains the computed magnetic moments of almost all cases. (The moment of a C at the Br-tetragonal site will be discussed in the next paragraph.) Note that for Br substitutional defects, the localized level gains one electron from the matrix since the system is Br deficient. We also note that the fact that magnetic moments change with different types of impurity atoms and charge states may enable electronic control of the magnetic moments.

Consider the case of C at the Br-tetragonal site. As shown in Fig. 7(a) the final local symmetry near the C interstitial is D_{2h} with the initial Br cubic square being distorted to a

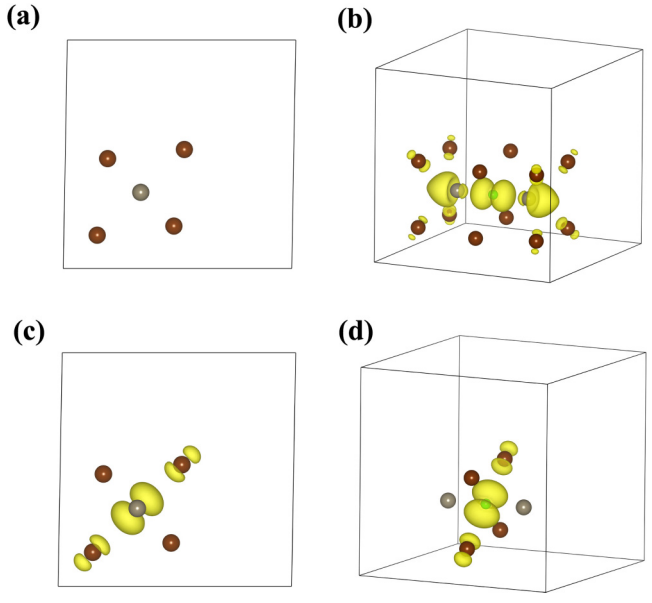

FIG. 7. (Color online) (a) Front view of relaxed atomic defect configuration for C at Br tetragonal. (b) Side view of the partial charge density contour of the second-highest state. (c) Front view and (d) side view of the partial charge density contour of the highest state.

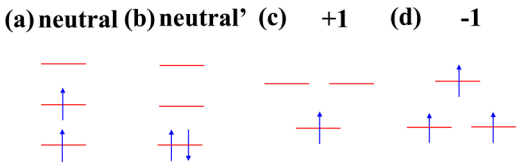

FIG. 8. (Color online) Electron filling diagrams of C at Br-tetragonal site: (a) ground state of neutral charge, (b) higher energy state of neutral charge, (c) ground state of $+1$ charge, and (d) ground state of -1 charge.

diamond shape. The partial charge density contours indicate that the two highest states have different symmetries. The second highest occupied state, shown in Fig. 7(b), has major distribution along the direction of two n.n. Tl ions. The highest occupied state, shown in Figs. 7(c) and 7(d), is aligned along the longer diagonal of Br diamond. Given that the calculated magnetic moments are 1.96 μ_B, we propose the electron filling diagram in Fig. 8(a). Two electrons fill two different levels with the same spin direction rather than fill the lowest level with opposite spins, as shown in Fig. 8(b).

We believe the reason for this is that the magnitude of the splitting is not large enough to compensate for the on-site Coulomb repulsion when two electrons try to fill the lowest level. We also studied the $+1$ and -1 charge states of this defect configuration. The electron filling diagrams in Figs. 8(c) and 8(d) are proposed according to the calculated magnetic moments and the symmetries of partial charge density plots. For the -1 charge state, the local environment retains a D_{4h} symmetry with four Br ions forming a square after relaxation (not the diamond in neutral charge state). The lower level is the 2-fold degenerate level. Two states of this level are aligned along the one and the other diagonals of Br square, respectively. The higher 1-fold level is aligned along two n.n. Tl ions. Three electrons fill three levels with same direction of spin. The reason for this is also to avoid large on-site Coulomb repulsion through the third electron occupying a slightly higher but empty level [Fig. 8(d)]. The calculated magnetic moments are 2.93 μ_B which is close to 3 μ_B from our model. For the $+1$ charge state, the local symmetry is also D_{4h}, but the distance from C to n.n. Br (2.52 Å) is smaller than that in the -1 charge state (3.34 Å). While the distance from C to n.n. Tl (2.55 Å) is close to that in the -1 charge state (2.36 Å). The partial charge density plot indicates the occupied state is aligned along the direction of two n.n. Tl ions. This means large local distortion flips the order of levels in the -1 charge state. Thus one p electron fills the lower 1-fold level and gives 1 μ_B magnetic moment, close to the calculated 0.99 μ_B [Fig. 8(c)]. The case of C at the Br-tetragonal site illustrates the deficiency of our model that it does not give the magnitude of the energy level splitting and the on-site Coulomb repulsion. A full understanding requires a more detailed model.

We have not computed absolute formation energies for the defects considered here. However, there is experimental proof that TlBr can be doped with C, N, and O [18]. We have computed relative formation energies for the defects and we find that for C, the most stable site is the nonmagnetic C_{2v} site. However, the formation energy of the C atom on the Tl-tetragonal site is approximately 0.25 eV greater. This

energy difference is not insurmountable from a processing perspective, and the calculations indicate that the C atom at the Tl-tetragonal site is metastable. This suggests that nonequilibrium occupation of the Tl-tetragonal sites might be stabilized, enabling the magnetism to be studied. In the case of N, the 2-fold site retains its magnetization. (A more complete discussion of defect concentration and relative formation energies may be found in the Supplemental Material [23].) We also have not considered the exchange coupling between the localized spins. Thus at this stage, we cannot comment on the global behavior of magnetism within the material.

In summary, we predict that traditionally nonmagnetic impurity atoms (C, N, and O) occupying certain high-symmetry sites of TlBr are magnetically polarized. We propose a simple model to show that the magnetic moments come from the p electrons of the impurity atoms. The model successfully explains the magnetic moments for a wide range of dopants, sites, and charge states.

This work was supported by the U.S. Department of Homeland Security under Grant Award No. 2009-DN-077-ARI-026-04 and by the Director, Office of Science, Office of Basic Energy Sciences, Division of Materials Sciences and Engineering, of the U.S. Department of Energy under Contract No. DE-AC02-05CH11231.

[1] T. Dietl, Nat. Mater. **9**, 965 (2010).
[2] J. K. Furdyna, J. Appl. Phys. **64**, R29 (1988).
[3] H. Munekata, H. Ohno, S. von Molnar, A. Segmüller, L. L. Chang, and L. Esaki, Phys. Rev. Lett. **63**, 1849 (1989).
[4] H. Ohno, A. Shen, F. Matsukura, A. Oiwa, A. Endo, S. Katsumoto, and Y. Iye, Appl. Phys. Lett. **69**, 363 (1996).
[5] H.-J. Lee, S.-Y. Jeong, C. R. Cho, and C. H. Park, Appl. Phys. Lett. **81**, 4020 (2002).
[6] A. L. Ivanovskii, Phys. Usp. **50**, 1031 (2007).
[7] S. Zhou, Q. Xu, K. Potzger, G. Talut, R. Grotzschel, J. Fassbender, M. Vinnichenko, J. Grenzer, M. Helm, H. Hochmuth, M. Lorenz, M. Grundmann, and H. Schmidt, Appl. Phys. Lett. **93**, 232507 (2008).
[8] H. Pan, J. B. Yi, L. Shen, R. Q. Wu, J. H. Yang, J. Y. Lin, Y. P. Feng, J. Ding, L. H. Van, and J. H. Yin, Phys. Rev. Lett. **99**, 127201 (2007).
[9] I. Slipukhina, Ph. Mavropoulos, S. Blügel, and M. Ležaić, Phys. Rev. Lett. **107**, 137203 (2011).
[10] M. Seike, V. A. Dinh, K. Sato, and H. K. Yoshida, Phys. B: Condens. Matter **407**, 2875 (2012).
[11] J. Nakahara, K. Kobayashi, and A. Fujii, J. Phys. Soc. Jpn. **37**, 1312 (1974).
[12] D. C. Hinson and J. R. Stevenson, Phys. Rev. **159**, 711 (1967).
[13] H. M. Smith, Y. Zhou, G. Ciampi, H. Kim, L. J. Cirignano, K. S. Shah, E. E. Haller, and D. C. Chrzan, Appl. Phys. Lett. **103**, 091901 (2013).
[14] A. Churilov, G. Ciampi, H. Kim, L. Cirignano, W. Higgins, F. Olschner, and K. Shah, IEEE Trans. Nucl. Sci. **56**, 1875 (2009).
[15] H. Kim, L. Cirignano, A. Churilov, G. Ciampi, W. Higgins, F. Olschner, and K. Shah, IEEE Trans. Nucl. Sci. **56**, 819 (2009).
[16] S. R. Bishop, W. Higgins, G. Ciampi, A. Churilov, K. S. Shah, and H. L. Tuller, J. Electrochem. Soc. **158**, J47 (2011).
[17] S. R. Bishop, H. L. Tuller, G. Ciampi, W. Higgins, J. Engel, A. Churilov, and K. S. Shah, Phys. Chem. Chem. Phys. **14**, 10160 (2012).
[18] H. M. Smith, Ph.D. thesis, University of California, Berkeley, 2013.
[19] G. Kresse and J. Hafner, Phys. Rev. B **47**, 558 (1993).
[20] J. P. Perdew, K. Burke, and M. Ernzerhof, Phys. Rev. Lett. **77**, 3865 (1996).
[21] G. Kresse and D. Joubert, Phys. Rev. B **59**, 1758 (1999).
[22] M. Ernzerhof and G. E. Scuseria, J. Chem. Phys. **110**, 5029 (1999).
[23] See Supplemental Material at http://link.aps.org/supplemental/10.1103/PhysRevB.89.195201 for discussions of the symmetry of the wave function and partial charge density, mathematical details, and the defect concentration and relative formation energies.
[24] For more information about the program, please refer to http://jp-minerals.org/vesta/en.